Clustering of fracture orientations using a mixed Bingham distribution and its application to paleostress analysis from dike or vein orientations

Atsushi Yamaji[a], Katsushi Sato[a]

[a] *Division of Earth and Planetary Sciences, Graduate School of Science, Kyoto University, Kyoto 606-8502, Japan*

Abstract

The clustering and classification of fracture orientations are important in rock mechanics and in brittle tectonics, the latter of which includes the paleostress analysis of extension fractures hosting dikes or mineral veins. Here, we present an unsupervised clustering method for the orientations of extension fractures using mixed Bingham distributions. The method not only detects the elliptical clusters and girdles made by the poles to such planar features, but also determines the appropriate number of those groups by means of Bayesian information criterion (BIC) without a priori information. The method was tested with artificial data sets, and successfully detected the assumed groups, when the clusters had little overlaps. However, clusters with the common maximum concentration orientation and large aspect ratios were distinguished, provided that their minimum concentration orientations were separated by a large angle. Our method separated two stress states from natural data from a Miocene dike swarm in SW Japan. The method also evaluated the probabilities of the stresses to form each of the dike.

Keywords: Bingham statistics, Bayesian information criterion, mixture model, cluster analysis, tectonic stress, dike, magma pressure

1. Introduction

The clustering of orientation data is important in various branches of science and engineering. Discontinuity orientations in rock material are carefully observed when surface and underground excavations are made from efficiency and safety standpoints (Priest, 1993). Their orientation distribution is important for wellbore stability (Chen et al., 2008) and groundwater hydrology (e.g., Panda and Kultilake, 1999; Ohtsu et al., 2008). Accordingly, various clustering techniques for the orientations have been proposed since the 1970s by researchers mainly in civil engineering (e.g., Shanley and Mahtab, 1976; Wallbrecher, 1978; Hammah and Curran, 1998, 1999; Peel et al., 2001; Marcotte and Henry, 2002; Klose et al., 2005; Jimenez-Rodriguez and Sitar, 2006). Dortet-Bernadet and Wicker (2008) suggest that Peel et al. (2001), who clustered rock joints, stimulated researchers in other fields of science to tackle the problem.

Such clustering is important for understanding brittle tectonics as well. The orientations of healed microcracks (Lespinasse and Pécher, 1986; Kowallis et al., 1987) and joints (Whitaker and Engelder, 2005) are thought to indicate paleostress orientations. In addition, dike and vein orientations are used to infer all the axes of the paleostress at the time of the vein or dike formation (Baer et al., 1994; Jolly and Sanderson, 1997; Yamaji et al., 2010). The clustering of vein orientations was used by Ahmadhadi et al. (2008) to infer the timing of folding. The clustering of fracture orientations has potential for investigating polyphase tectonics.

Fault-slip analysis has been used to study polyphase tectonics (e.g., Etchecopar et al., 1981; Nemcok and Lisle, 1995; Yamaji, 2000; Shan et al., 2003; Sato, 2006; Yamaji et al., 2006). The fault-slip data resulting from such tectonics is called heterogeneous. Likewise, we call a data set heterogeneous, if the data are collected from from the fractures that should be classified into some groups with different origins.

In this paper we present a clustering method for dealing with heterogeneous orientation data. It is assumed that the poles to planar features of the same origin make an elliptical cluster or a girdle that is approximated by a Bingham distribution (Bingham, 1974). This is the simplest orientation distribution to delineates them (Fig. 1), and is easily related with the dilation of fractures by overpressured fluids (Baer et al., 1994; Jolly and Sanderson, 1997; Yamaji et al., 2010). Our method simultaneously fits a few Bingham distributions to a set of heterogeneous data. That is, a mixed Bingham distribution is fitted to them. Our numerical technique not only detects and separates the clusters and girdles, but also determines their number from the orientation data themselves. The method was tested with artificial data sets to demonstrate its resolution, and with natural data sets from a dike swarm.

The analysis of clustering of dike orientations and vein orientations will stimulate structural geologists and researchers in related areas. Once fractures are classified, radiometric dating, paleomagnetic, petrological and geochemical analyses, etc., of the members of each class shed new light on the formation of the dike and vein clusters and on their tectonic, volcanological and hydrological implications.

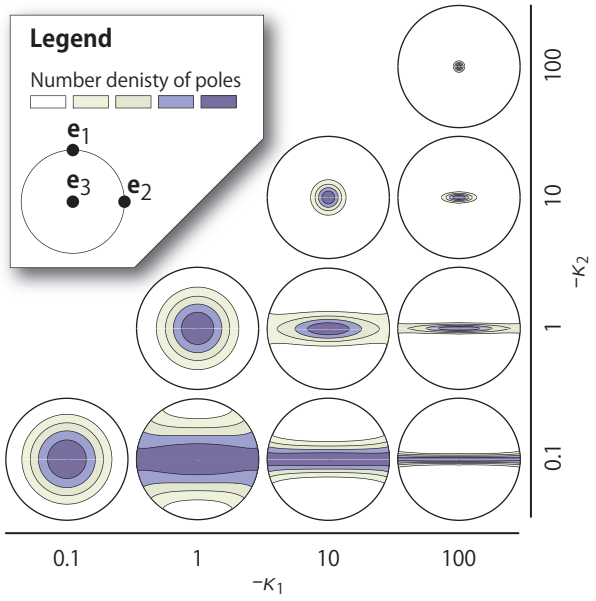

Figure 1: Equal-area projections showing the probability densities of the Bingham distributions with different κ_1 and κ_2 values, both of which are negative in sign. The distributions have orthorhombic symmetry, meaning that they are symmetric with respect to the planes perpendicular to the unit vectors, $\mathbf{e}_1$, $\mathbf{e}_2$ or $\mathbf{e}_3$. Note that the stereograms have different contour intervals: the range between the minimum and maximum densities, i.e., $\mathcal{P}_{\mathrm{B}}(\mathbf{e}_1|\mathbf{K},\mathbf{E})$ and $\mathcal{P}_{\mathrm{B}}(\mathbf{e}_3|\mathbf{K},\mathbf{E})$, is divided into 5 intervals.

2. Bingham and mixed Bingham distributions

The Bingham distribution is the simplest extension of the multivariate normal distribution to the three-dimensional orientation distribution of lines (e.g., Love, 2007). It is convenient to consider antipodally distributed points on a sphere to represent the lines that meet at the center of the sphere. The Bingham distribution is depicted by a girdle or an elliptical cluster of such points.

An elliptical cluster or a girdle has orthorhombic symmetry if it is described by the Bingham distribution. That is, it has the three symmetry axes that meet at right angles; two of them indicate the orientations of maximum and minimum concentrations. The remaining axis is known as the orientation of intermediate concentration. Following Love (2007), we use the unit column vectors, $\mathbf{e}_1$, $\mathbf{e}_2$ and $\mathbf{e}_3$, to refer to the orientations of the minimum, intermediate and maximum concentrations, respectively (Table 1). The cluster center is represented by $\mathbf{e}_3$, which is identified with the σ_3-axis in section 5 (Baer et al., 1994; Jolly and Sanderson, 1997; Yamaji et al., 2010).

The paired parameters, κ_1 and κ_2, distinguish uniform, elliptical and girdle distributions (Fig. 1): They are negative in sign, and their absolute values, $|\kappa_1|$ and $|\kappa_2|$, indicate the concentration of data points from $\mathbf{e}_3$ to $\mathbf{e}_1$ and from $\mathbf{e}_3$ to $\mathbf{e}_2$, respectively, on the sphere. A uniform distribution is indicated by $\kappa_1 = \kappa_2 = 0$. Circular and elliptical distributions are indicated by $\kappa_1 = \kappa_2 < 0$ and $\kappa_1 < \kappa_2 < 0$, respectively. Girdle distributions are denoted by the parameters that satisfy $\kappa_1 \ll \kappa_2 \lessapprox 0$.

If points on a unit sphere obey Bingham distribution, they have the probability density (Love, 2007)

$$\mathcal{P}_{\mathrm{B}}(\mathbf{v}\,|\,\mathbf{K},\mathbf{E}) = \frac{1}{A}\exp\left(\mathbf{v}^{\top}\mathbf{E}^{\top}\mathbf{K}\mathbf{E}\mathbf{v}\right),$$

where $\mathbf{v}$ is the unit vector representing an orientation, A is the normalization constant, $\top$ indicates matrix transpose, $\mathbf{E} = (\mathbf{e}_1, \mathbf{e}_2, \mathbf{e}_3)$ is the orthogonal matrix representing the attitude of the Bingham distribution, and $\mathbf{K} = \mathrm{diag}(\kappa_1, \kappa_2, 0)$. The distribution has five degrees of freedom: three for the orthonormal vectors, $\mathbf{e}_1$, $\mathbf{e}_2$ and $\mathbf{e}_3$, and two for the concentration parameters. Accordingly, the parameters of the distribution are represented by a position vector, $\mathbf{x}$, in a five-dimensional parameter space (Appendix A). That is, the paired parameters, $\{\mathbf{K},\mathbf{E}\}$, have a one-to-one correspondence with a point in the space. We refer $\mathcal{P}_{\mathrm{B}}(\mathbf{v}\,|\,\mathbf{x})$ to the probability density of the Bingham distribution with the parameters that are denoted by $\mathbf{x}$.

The Bingham distribution is so flexible as to denote either an elliptical cluster or a girdle made by the poles to fractures. Accordingly, it is useful to assume that a heterogeneous set of orientation data obeys the mixed Bingham distribution, which has the probability density

$$\mathcal{P}_{\mathrm{mB}}(\mathbf{v}\,|\,\boldsymbol{\theta},\boldsymbol{\varpi}) = \sum_{k=1}^{K}\varpi^k\mathcal{P}_{\mathrm{B}}(\mathbf{v}\,|\,\mathbf{x}^k), \tag{1}$$

where K is the number of elliptical clusters or girdles, ϖ^k is the compounding ratio or the mixing coefficient (Bishop, 2006) of the kth Bingham distribution of which parameters are represented by $\mathbf{x}^k$. The coefficients satisfy $0 < \varpi^k \leq 1$ and $\varpi^1 + \cdots + \varpi^K = 1$: ϖ^k means the significance of the kth subset. The argument, $\boldsymbol{\theta}$, of the function $\mathcal{P}_{\mathrm{mB}}(\,)$ in Eq. (1) stands for all the K vectors:

$$\boldsymbol{\theta} = \left\{\mathbf{x}^1, \mathbf{x}^2, \ldots, \mathbf{x}^K\right\}, \tag{2}$$

and another argument of the function is $\boldsymbol{\varpi} = \{\varpi^1, \varpi^2, \ldots, \varpi^K\}$. Fig. 2 shows an example with the parameters, $K = 2$, $\varpi^1 = 0.4$ and $\varpi^2 = 0.6$. Fig. 3a shows the artificial data made from the mixed Bingham distribution with three Bingham components ($K = 3$). The orientations generated from the first, second and third components are distinguished by symbols, i.e., triangles, circles and squares, respectively, on the equal-area projection.

Our task is the unsupervised clustering (e.g., Tan et al., 2005) of the orientations. That is, in the case of Fig. 3a, it is required to group the orientations into three by the orientations themselves under the condition that the distinction of the symbols is masked.

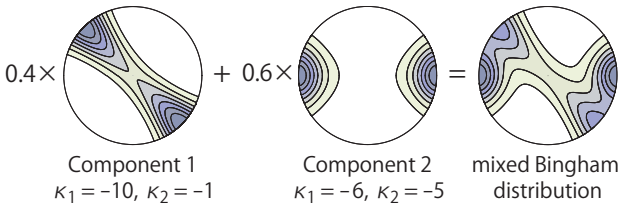

Figure 2: Equal-area projections showing probability densities of the Bingham components 1 and 2, and their mixture with the mixing coefficients 0.4 and 0.6.

Table 1: List of symbols. Superscript at the upper left and upper right of a symbol denote, respectively, the number of iterations in the EM algorithm and the consecutive number of Bingham components in a mixed Bingham distribution. Circumflex accents indicate the quantities of the mixed Bingham distribution optimized for a data set.

BIC	Bayesian information criterion
$\mathbf{E}$	orthogonal matrix representing the symmetry axes of a Bingham distribution
$\mathbf{e}_1$	the minimum concentration axis of a Bingham distribution
$\mathbf{e}_2$	the intermediate concentration axis of a Bingham distribution
$\mathbf{e}_3$	the maximum concentration axis of a Bingham distribution
K	the number of Bingham component of a mixed Bingham distribution
$\mathbf{K}$	diagonal matrix with the diagonal components, κ_1, κ_2 and 0
$\mathcal{L}(\,)$	logarithmic likelihood function
N	the number of data
$\mathcal{P}_{\mathrm{B}}(\,)$	probability density function of Bingham distribution
$\mathcal{P}_{\mathrm{mB}}(\,)$	probability density function of mixed Bingham distribution
$\mathbf{v}$	unit vector normal to a fracture plane
$\mathbf{v}_n$	$\mathbf{v}$ of the nth fracture
$\mathbf{x}$	a five-dimensional vector representing a Bingham distribution
z_n^k	the membership of the nth datum to the kth Bingham component or the responsibility of the kth one for the nth datum
$\boldsymbol{\theta}$	the set of the K vectors representing Bingham distributions
κ_1, κ_2	concentration parameters of a Bingham distribution ($\kappa_1 \le \kappa_2 \le 0$)
$\boldsymbol{\varpi}$	the set of K mixing coefficients
ϖ^k	the mixing coefficient of the kth Bingham component
σ_1, σ_2, σ_3	principal stresses ($\sigma_1 \ge \sigma_2 \ge \sigma_3$)
Φ	stress ratio

3. Clustering

Given heterogeneous orientation data, we determine the mixed Bingham distribution (Eq. 1) that best fits the data. Each Bingham component represents a homogeneous subset. The goodness of fit is evaluated by the logarithmic likelihood function,

$$\mathcal{L}(\boldsymbol{\theta}, \boldsymbol{\varpi}) = \sum_{n=1}^{N} \log_{\mathrm{e}} \mathcal{P}_{\mathrm{mB}}(\mathbf{v}_n \,|\, \boldsymbol{\theta}, \boldsymbol{\varpi}), \tag{3}$$

where $\mathbf{v}_n$ is the unit vector indicating the nth datum, N is the number of data. The mixed distribution that best fits the N data is given by the optimal parameter set, $\{\hat{\boldsymbol{\theta}}, \widehat{\boldsymbol{\varpi}}\}$, that maximizes this function. The optimization of the parameter set is performed using the expectation-maximization (EM) algorithm (e.g., Bishop, 2006) from the following initial conditions.

Initial conditions. The EM algorithm starts from the initial parameter set, ${}^0\boldsymbol{\theta}$, where the superscript refers to the ordinal number of iterations. K points are casted randomly around the origin of the parameter space to make the initial vectors, ${}^0\mathbf{x}^1, \ldots, {}^0\mathbf{x}^K$ that fill up ${}^0\boldsymbol{\theta}$ (Eq. 2). This parameter is improved through the following E- and M-steps. The optimal parameter set, $\{\hat{\boldsymbol{\theta}}, \widehat{\boldsymbol{\varpi}}\}$, at the time the algorithm is terminated depends on the initial conditions. Accordingly, the EM algorithm was started with different initial conditions more than 100 times to optimize the parameter set.

E-step. If data were obtained from a mixure of K fracture sets with different origins, each datum should belong to one of the clusters or the girdles corresponding to the K sets. Let z_n^k be the membership of the nth datum to the kth set. This is exactly expressed by the binary attributes 0 and 1 as $z_n^1 = \cdots = z_n^{k-1} = 0$, $z_n^k = 1$ and $z_n^{k+1} = \cdots = z_n^K = 0$. However, we do not know which of the K sets the nth datum should be assigned to. Therefore, the validity for the nth datum to belong to the kth set with the parameter ${}^i\mathbf{x}^k$ is estimated not exactly but fuzzily as

$${}^i z_n^k = \frac{\mathcal{P}_{\mathrm{B}}(\mathbf{v}_n \,|\, {}^i\mathbf{x}^k)}{\sum_{k=1}^{K} \mathcal{P}_{\mathrm{B}}(\mathbf{v}_n \,|\, {}^i\mathbf{x}^k)}. \tag{4}$$

The left-hand side of this equation is called the responsibility of the kth one for the nth datum or the membership of the datum to the kth group, and satisfies $0 \le {}^i z_n^k \le 1$. In case of $K = 2$, the nth datum belongs to the first and second groups at the probabilities of, say, 10% and 90%, respectively. Then, the mixing coefficients are updated in this step as ${}^i\varpi^k \propto {}^i z_1^k + \cdots + z_N^k$, where the constant of proportionality is given by the normalization condition, ${}^i\varpi^1 + \cdots + {}^i\varpi^K = 1$. The set, ${}^i\boldsymbol{\varpi}$, is composed of those coefficients.

M-step. Keeping ${}^i\boldsymbol{\varpi}$ unchanged, ${}^i\boldsymbol{\theta}$ is improved to ${}^{i+1}\boldsymbol{\theta}$ by the numerical maximization of the logarithmic likelihood function (Eq. 3). The simplex method (Nelder and Mead, 1965) was used for this purpose.

Termination condition. The parameter set, $\{\boldsymbol{\theta}, \boldsymbol{\varpi}\}$, is gradually improved by shuttling the E- and M-steps for the mixed Bing-

ham distribution to approximate the given data. This iterative process is terminated when the improvement of $\{\boldsymbol{\theta}, \boldsymbol{\varpi}\}$ becomes small. That is, the termination condition, $\left|{}^{i}\mathcal{L} - {}^{i-1}\mathcal{L}\right| / {}^{i-1}\mathcal{L} < 10^{-6}$, is used for this purpose, where ${}^{i-1}\mathcal{L}$ and ${}^{i}\mathcal{L}$ are the values of the logarithmic likelihood function (Eq. 3) at the end of the $(i-1)$th and ith M-step, respectively. We refer to the parameter set optimized for the data as $\hat{\boldsymbol{\theta}}$ and $\widehat{\boldsymbol{\varpi}}$. Likewise, if necessary, the optimal quantities are indicated by circumflex accents such as $\hat{z}_n^k$, etc.

Number of components. Given a data set, the goodness of fit (Eq. 3) is generally improved by the increasing number of components, K. However, every data set includes random errors. It is meaningless to fit the mixed distribution to erroneous data: this makes the inferred mixed distribution too complex. In addition, it is usually difficult to describe entire fracture orientations in a rock body in question. Biased observation can make it happen that two or three clusters appear from the fracture orientations that actually make a girdle. Accordingly, it is important to estimate an appropriate K value from data themselves in a statistical sense. This is accomplished by using

$$\mathrm{BIC} = -2\mathcal{L}(\hat{\boldsymbol{\theta}}, \widehat{\boldsymbol{\varpi}}) + (6K-1)\log_{\mathrm{e}} N,$$

called the Bayesian information criterion (Schwarz, 1978). The right-hand side of this equation is evaluated from data and an assumed K value: The coefficient $(6K-1)$ is the degree of freedom of the mixed Bingham distribution with K components. The final term in this equation is the penalty against increasing components. The best K value minimizes BIC. That is, BICs are evaluated for various K values, and the value corresponding to the minimum BIC is chosen as the best. The mixed Bingham distribution with the best K value is thought to be the optimal mixture model for the given data.

4. Test

The present method was tested, first, with artificial data sets. To this end, orientations obeying Bingham distributions were generated using the rejection method (e.g., Press et al., 2007), and were combined to make a data set. The sample data sets were generated with the assumed values of K, $\boldsymbol{\theta}$ and $\boldsymbol{\varpi}$. The method was tested with the data if the values were restored only from the data.

4.1. Number of components

We tested the present method, first, with the data in Fig. 3a to see if BIC works. The data set was made of 60-, 40- and 40-element subsets. As a result, the correct number of the subsets was obtained by minimizing BIC. There are three distinctive clusters in Fig. 3a. Therefore, if we do not know the method of data generation, three seems the appropriate value for K. The best K value, which is indicated by the minimum value of BIC, was consistent with this intuition (Fig. 3c). For K greater than 3, the three clusters were unnecessarily subdivided into two or more groups (Fig. 3b).

When three components were assumed ($K = 3$), the symmetry axes of the Bingham components were accurately located (Fig. 3a). But, the mixing coefficients $\widehat{\varpi}^1$ and $\widehat{\varpi}^2$ were slightly under- and over-estimated, respectively (Fig. 3c), because the peripheral parts of the corresponding clusters overlapped with each other. In contrast, $\widehat{\varpi}^3$ was accurately evaluated, as the cluster of the third component was clearly separated from the other clusters.

The membership of the nth datum to the first, second and third Bingham components, $\hat{z}_n^1$, $\hat{z}_n^2$ and $\hat{z}_n^3$, are depicted by the color hue of the symbols plotted on the stereogram in Fig. 3a. It follows from Eq. (4) that the memberships of the nth datum satisfy $\hat{z}_n^1 + \hat{z}_n^2 + \hat{z}_n^3 = 1$. Therefore, the ternary diagram in this subfigure is used to depict the correspondence between a color and a triplet of the memberships. Most of the data points in Fig. 3a have one of the primary colors, red, green and blue, indicating that the separation of the data set into homogeneous subsets was almost perfect. A few exceptions to this appeared in the peripheral part of the first subset where the first and second subsets overlapped. There are a few green triangles in Fig. 3a, indicating misclassified data. In contrast, all the data from the third Bingham component were correctly classified into the third class ($z_n^3 \approx 1$).

When four components were assumed ($K = 4$), the third cluster was divided into two: the fourth one was located at the densest part of the third cluster. In this case, the memberships satisfy $\hat{z}_n^1 + \hat{z}_n^2 + \hat{z}_n^3 + \hat{z}_n^4 = 1$. It follows that, in the same way as the case of $K = 3$ where a ternary plot indicates memberships, a quartet of the memberships in the case of $K = 4$ are represented by a point in or on the surface of a regular tetrahedron. So, the quartets are denoted by a colored tetrahedron in Fig. 3b. Its four vertices indicate the permutations, $[1,0,0,0]$, $[0,1,0,0]$, $[0,0,1,0]$ or $[0,0,0,1]$, where the first through fourth memberships are bracketed. These are indicated by red, green, blue and black, respectively, in the subfigure.

The symmetry axes, mixing coefficients and responsibilities were accurately evaluated, but the optimal values of κ_1 and κ_2 were less accurate than them. The open circles and crosses in Fig. 3e show that the parameters were determined with the errors of 10–20%. This is because the parameters were determined from minute differences in the elongation and spread of the clusters.

4.2. Resolution

The next test was made for investigating the resolution of the method using a suite of artificial data sets with the two Bingham components that were generated by the procedure in Fig. 4. Data of the component 1 were rotated about the horizontal E–W orientation and mixed with those of the component 2. The rotation angle ψ was increased from 0° to 90° with the interval of 10° to see if the method can separate them. The smaller the angle, the more difficult it is to separate the components from a mixed data set. Figs. 5, 6 and 7 show the results.

It was found that the two components were separated successfully for $\psi \gtrapprox 40°$. This is demonstrated by the graphs of BIC in Fig. 6. The angle of this threshold angle is not surprising because the clusters of both the components have the half

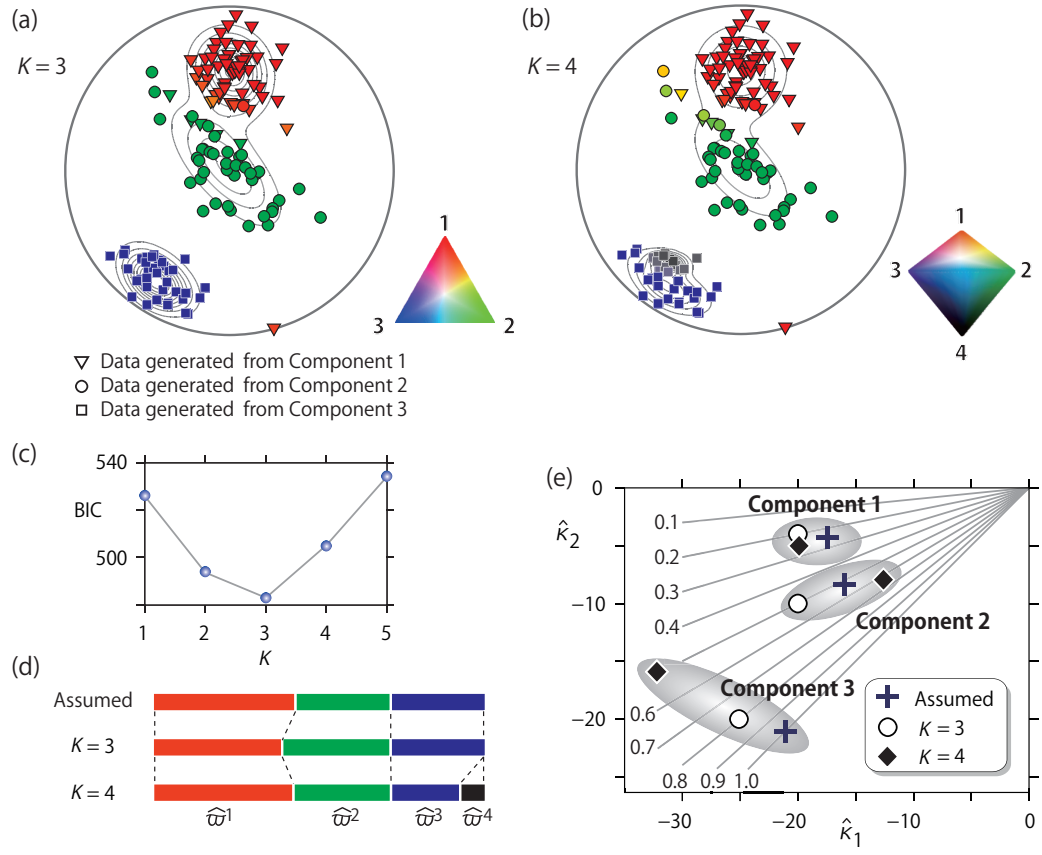

Figure 3: Artificial data generated from the mixed Bingham distribution with three components. The data should be classified into 60-, 40- and 40-element subsets, the distinction of which are indicated by triangles, circles and squares. (a) Equal-area projection showing the data set. In this case, three components ($K = 3$) were assumed. Therefore, the membership of each datum is depicted by a color in the ternary plot. Contours show the values of $\mathcal{P}_{\mathrm{mB}}(\hat{\boldsymbol{\theta}}, \widehat{\boldsymbol{\varpi}})$. (b) Equal-area projection showing the optimal mixture model for the case of $K = 4$ by the contours and by the memberships of data. The tetrahedron with red, green, blue and black vertices indicate the correspondence of the memberships with colors. (c) The BIC versus K, showing the prominent minimum at $K = 3$. (d) The optimal mixing ratios for the cases of $K = 3$ and 4. The third subset was erroneously subdivided into two in the latter case. (e) Assumed and optimal concentration parameters. Those of the component 4 for $K = 4$ were $\hat{\kappa}_1^4 = -158$ and $\hat{\kappa}_2^4 = -63$. Solid lines with the labels from 0.1 through 1.0 are the contours the ratio $\hat{\kappa}_2/\hat{\kappa}_1$.

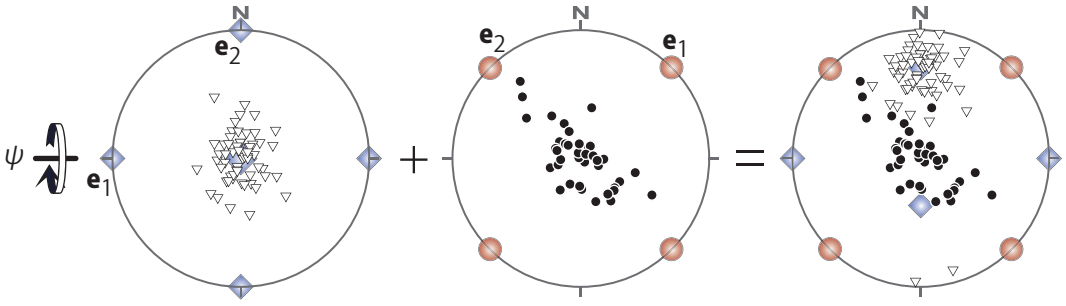

Figure 4: Equal-area projections illustrating the method of generating artificial data sets. Subsets 1 and 2 were generated from the Bingham distributions whose the parameters are shown under the stereoplots. Both the groups have the maximum concentration orientations in common. The orientations of Subset 1 were rotated about the $\mathbf{e}_1$-axis of the subset by the angle of ψ and mixed with those of Subset 2 to make a mixed Bingham distribution. The orientations from Subsets 1 and 2 are denoted by triangles and closed circles, respectively. Ten data sets were generated in this way with $\psi = 0, 10, \ldots, 90°$.

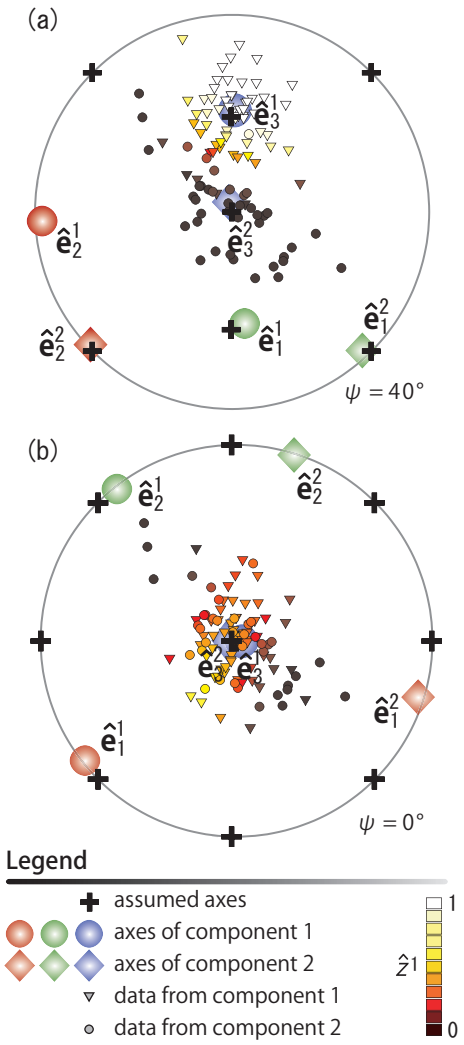

Figure 5: Equal-area projections showing the mixed Bingham distributions generated through the procedure of Fig. 4 with $\psi = 40°$ and $0°$. Bold crosses denote the symmetry axes that were used to generate the artificial data. The optimal stress axes and memberships were obtained with $K = 2$. The $\hat{z}^1$ value of each orientation datum is indicated by color gradation. That is, if triangles and circles in the stereoplots are painted black and white, respectively, the mixed data are separated into the correct two classes.

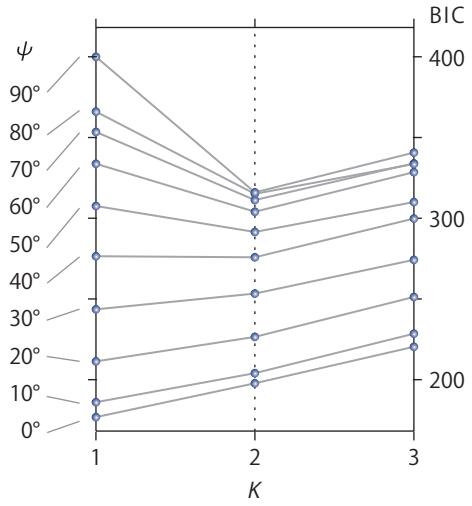

Figure 6: The BIC versus K for the artificial data sets generated in the way illustrated in Fig. 4 with the angles, $\psi = 0, 10, \ldots, 90°$. The BIC shows the minimum at $K = 2$ for $\psi \gtrapprox 40°$.

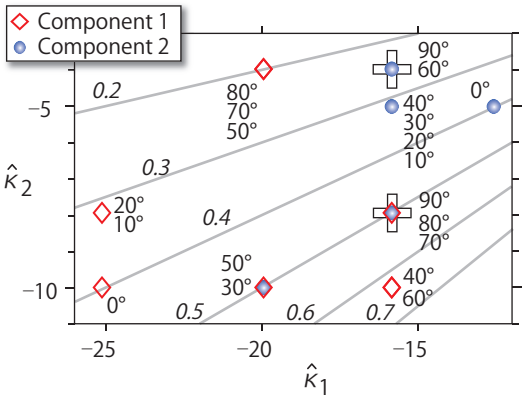

Figure 7: The concentration parameters of the mixed Bingham distributions that best fit the data sets with the ψ values from $0°$ through $90°$. Crosses denote the assumed values. Gray lines with the labels from 0.2 through 0.7 are the contours of the ratio $\hat{\kappa}_1/\hat{\kappa}_2$.

widths of about 20° (Figs. 4 and 5a). The clusters were easily resolved if ψ was greater than the summation of the half widths. The orientation data on the borders of the clusters had intermediate memberships, which are depicted by red to yellow in Fig. 5a.

Since the first component had an oval cluster with a relatively small aspect ratio, $\mathbf{e}_1$- and $\mathbf{e}_2$-axes were determined with errors larger than those of the second component. The cluster of the latter was so elongated that its three axes were accurately determined even for $\psi < 20°$. The misfit of the determined axes from the assumed ones was less than 10° for $\psi = 0°$ (Fig. 5b). In contrast, the determination of the concentration parameters was difficult and the results were unstable. Even for the cases of $\psi > 40°$, the $\hat{\kappa}_1$ and $\hat{\kappa}_2$ values deviated from the assumed values (Fig. 7).

Even when two clusters have common maximum concentra-

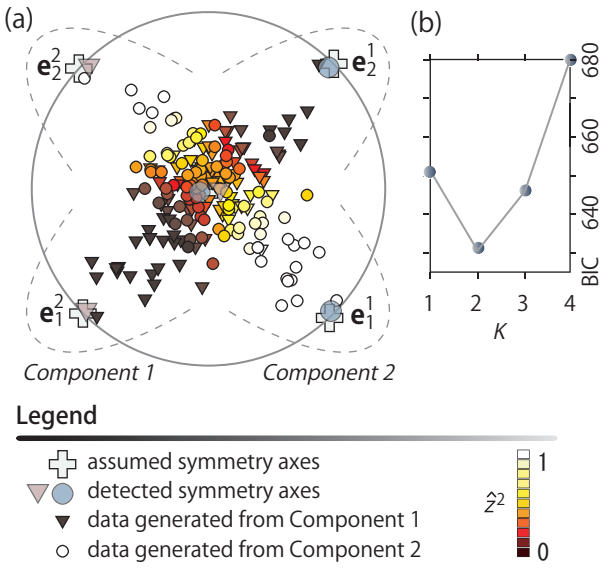

Figure 8: (a) Equal-area projection demonstrating the possibility of separating the two Bingham components that have the maximum concentration orientations in common. Their $\mathbf{e}_2$ orientations meet at a right angle. (b) BIC versus K for the mixed data in (a).

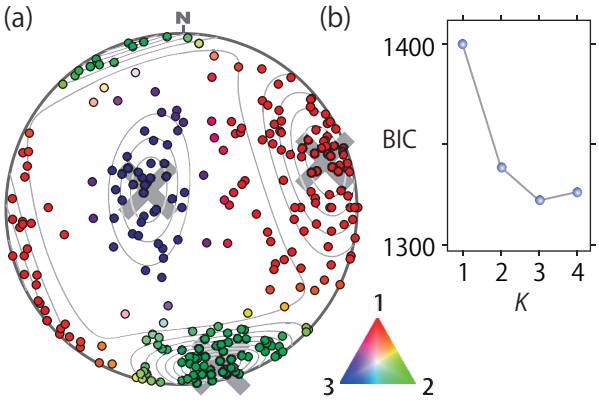

Figure 9: The benchmark test of the present method using the fracture orientation data from San Manual Copper mine, Arizona (Shanley and Mahtab, 1976). (a) The clustering result for the case of $K = 3$. Crosses denote the cluster centers, and the probability distribution of the mixed Bingham distribution optimal for the data is shown by contours. Equal-area, lower-hemisphere projection. (b) The BIC of the data shows the minimum at $K = 3$, indicating that the appropriate number of partitions was 3.

tion orientations, the Bingham components corresponding to the clusters can be accurately separated from mixed data in some cases. Fig. 8 shows an example, where the two Bingham components, each of which had 100 data, had elongated clusters with the $\mathbf{e}_2$-axis (elongation axis) making a right angle. The assumed mixing coefficients were $\varpi^1 = \varpi^2 = 0.50$. The optimal mixture model had the coefficients $\widehat{\varpi}^1 = 0.55$ and $\widehat{\varpi}^2 = 0.45$, indicating roughly correct separation. In addition, the BIC exhibited a prominent minimum correctly at $K = 2$. The method succeeded in separating the Bingham components. In this case, the success was due to the conditions: (1) both the components had large enough number of data, and (2) the elongated clusters had the intermediate concentration orientations separated by a large enough angle. Orientation data in the overlapping part of the two clusters had intermediate memberships, but those away from the overlapping part had the extreme values $\hat{z}^2 \approx 0$ or 1.

4.3. Application to natural data

The present method was applied to the orientation data from 286 fracture surfaces in San Manual copper mine, Arizona (Shanley and Mahtab, 1976), because the data set has been used as a benchmark of clustering techniques (Klose et al., 2005; Jimenez-Rodriguez and Sitar, 2006). Equal-area projection of the data clearly shows three clusters (Shanley and Mahtab, 1976) (Fig. 9a). Since the cluster centers were separated by ~90°, it was easy for our method to capture the clusters (Table 2).

The BIC of the San Manual data set demonstrated that three was the most adequate number of clusters for the data (Fig. 9b). There are a small number of data points with intermediate colors in Fig. 9a, indicating the clear separation of the data into three groups. In case of $K = 4$, such data points appeared along the base circle of the stereo plot, resulting in a larger BIC value.

Table 2: The parameters of the clusters detected from the San Manual data set by the present method (Fig. 9).

	Cluster 1	Cluster 2	Cluster 3
$\hat{\mathbf{e}}_1$	259° / 75°	040° / 75°	092° / 16°
$\hat{\mathbf{e}}_2$	162° / 02°	258° / 12°	184° / 08°
$\hat{\mathbf{e}}_3$	071° / 15°	166° / 09°	300° / 72°
$\hat{\kappa}_1$	−5.0	−15.8	−12.6
$\hat{\kappa}_2$	−3.2	−6.3	−4.0
$\widehat{\varpi}$	0.52	0.30	0.18

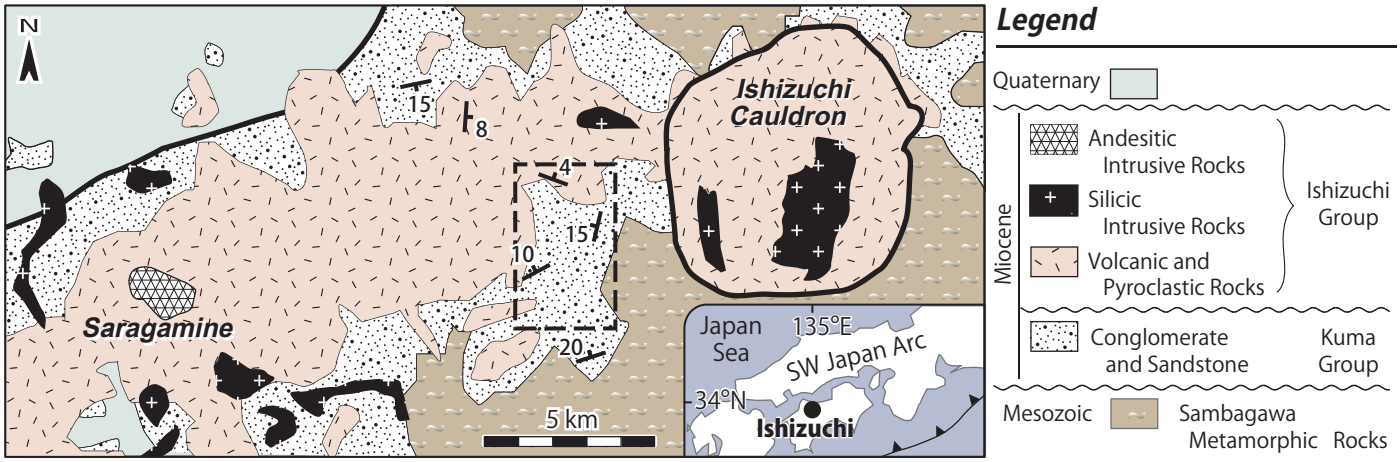

Figure 10: Geologic map of around the Ishizuchi area, Southwest Japan, simplified from Yoshida (1984). Dotted line shows the area where the attitudes of dikes were measured by Kusushashi and Yamaji (2001).

5. Paleostress analysis of dike or vein orientations

5.1. Method

Bingham distributions or the orientation distribution with orthorhombic symmetry were applied to dike orientations by Baer et al. (1994) and Jolly and Sanderson (1997) to infer the state of stress when the dikes were formed. The Jolly-Sanderson method was applied not only to igneous dikes but also to mineral veins (e.g., André et al., 2001; Mazzarini and Isola, 2007; Yamaji et al., 2010). Those authors identified the symmetry axes of the distribution, $\mathbf{e}_1$, $\mathbf{e}_2$ and $\mathbf{e}_3$, with the σ_1-, σ_2- and σ_3-axes, respectively. Recently, Yamaji et al. (2010) showed that the stress ratio, $\Phi = (\sigma_2 - \sigma_3)/(\sigma_1 - \sigma_3)$, of the stress state that affected the formation of epithermal veins could be approximated by the ratio of the concentration parameters, κ_2/κ_1.

Accordingly, when a mixed Bingham distribution is fitted to the orientation distribution of dikes or veins, we interpret the symmetry axes of each Bingham component as the principal axes of the paleostress that affected the formation of the dikes or veins corresponding to the data that have the highest memberships to the component. And, the concentration parameters are converted to stress ratios.

It is not surprising that factors including fluctuation in the state of stress, interactions among fractures, etc., lead to the errors of stress axes by ~10° in paleostress analysis. The difference of principal orientations at this level corresponds to a ~0.2 difference in stress ratio (Yamaji and Sato, 2006). Therefore, we should be tolerant of uncertainty in the ratio at around 0.2. In addition, the ratio is determined less accurately than stress axes, because the errors of the concentration parameters propagate to that of the ratio (Figs. 3e and 7).

5.2. Application to natural data

The present method was applied to the natural data from Miocene andesitic dikes in the Ishizuchi area (Nagai and Horikoshi, 1955), Southwest Japan (Fig. 10). They are called the Kuromoritoge dike swarm (Yoshida et al., 1993), and were found in the Lower Miocene Kuma Group and the coeval volcanic rocks. At the time they intruded, the volcanic center existed under Mount Saragamine just before the collapse event to form the Ishizuchi cauldron at ~15 Ma (Yoshida, 1984). We use the orientation data from the 37 dikes reported by Kusushashi and Yamaji (2001). Fig. 11 shows the data and the result.

We found that the data were explained by the mixture of two Bingham distributions: BIC of the data showed the minimum at $K = 2$ (Fig. 11b). The two cluster centers in the stereogram were located in the SSW and NNW directions. The stress state corresponding to the former, referred to as Stress A, had the values $\widehat{\varpi} = 0.69$, $\hat{\kappa}_1 = -12.6$, $\hat{\kappa}_2 = -4.00$ and $\hat{\Phi} = 0.32$. The second cluster represents Stress B with the parameters $\widehat{\varpi} = 0.31$, $\hat{\kappa}_1 = -79.4$, $\hat{\kappa}_2 = -6.3$ and $\hat{\Phi} = 0.08$.

Both the stress states had σ_3-axes that meet the trend of the Southwest Japan arc at angles greater than ~60°. The roughly arc-perpendicular σ_3-orientations are consistent with the interpretation that the magmatism in the Ishizuchi area began in the final stage of back arc opening in the Japan Sea (Kobayashi, 1979; Yoshida, 1984; Yamaji and Yoshida, 1998; Kusushashi and Yamaji, 2001). Stress B was possibly the regional extensional tectonics. Local factors, i.e., the topographic loading of volcanoes and the pressure from a magma chamber may have affected Stress A, which had a westerly plunging σ_1-axis. Mt. Saragamine is thought to have been the volcanic center at the time of dike intrusion (Yoshida, 1984). The plane defined by the σ_1- and σ_2-axes of Stress A runs roughly through the study area and Mt. Saragamine, suggesting the effect of magma pressure.

Similar stresses were found independently from mesoscale faults in the Kuma Group, a non-marine sedimentary package older than the dike swarm by a few million years. Fault-slip data were collected in the same area (dashed line in Fig. 10) by Kusushashi and Yamaji (2001). Fig. 11c shows the result of the multiple inverse method (Yamaji, 2000), where clusters on stereograms represent the stresses significant for the data. Namely, stresses with nearly vertical and westerly inclined σ_1-

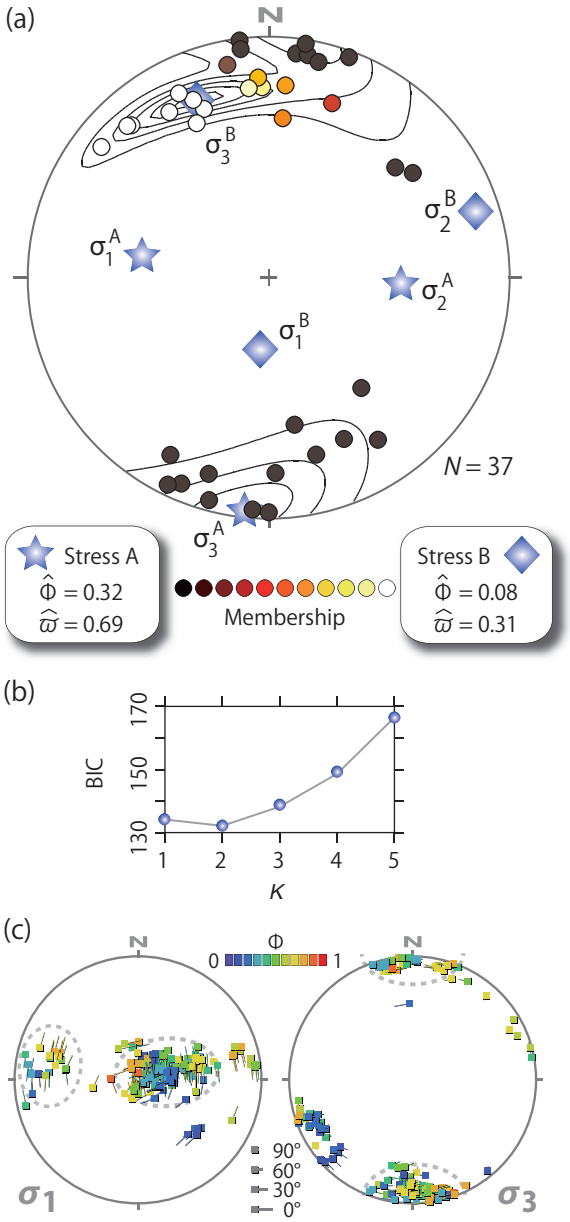

Figure 11: Result of the present method applied to the 37 dike orientations obtained at the western flank of the Ishizuchi Cauldron (Fig. 10). (a) Lower-hemisphere, equal-area projection. The principal axes of Stresses A and B inferred from the orientations are indicated by stars and diamonds, respectively. Solid lines are the contours of the theoretical probability density of the mixed Bingham distribution that best fit the data. Memberships of the data points are denoted by the gradation between black and white circles. (b) BIC versus K for the Ishizuchi data. (c) The σ_1- and σ_3-axes of the paleostresses determined by the multiple inverse method (version 5) (Yamaji, 2000) from the fault-slip data obtained in the same area by Kusushashi and Yamaji (2001). The data were collected from the Kuma Group (Fig. 10). Dotted lines highlight the clusters of stress tensors possibly corresponding to the stresses in (a). Paired stereograms show the σ_1- and σ_3-axes of stress tensors inferred from the data. Lower-hemisphere, equal-area projections.

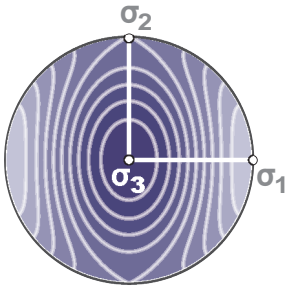

Figure 12: Contours on an equal-area projection show normal stress magnitudes acting on planes with various orientations. In this case, Φ is assumed to be 1/2. This pattern is symmetric with respect to the principal stress planes.

axes were found, and both the stresses had horizontal σ_3-axes. The principal orientations are similar to those inferred from the dikes.

The purpose of this subsection is to test the method with a natural data set, and to see if it leads to geologically relevant results. The tectonic and volcanological implications of the dikes should be drawn from increased data.

6. Discussion

Several numerical methods have been proposed for clustering fracture orientations (Shanley and Mahtab, 1976; Pecher, 1989; Hammah and Curran, 1998; Peel et al., 2001). Klose et al. (2005), Jimenez-Rodriguez and Sitar (2006) compared some of the methods and their own ones using the San Manual data (Fig. 9). All the methods determined cluster centers in similar orientations for $K = 3$.

Unlike those techniques, the present method aims not only at clustering orientation data but also at paleostress analysis of dikes and mineral veins. If a group of dikes or mineral veins were formed in fractures dilated by overpressured fluids, the variation in fracture orientations enables us to estimate the state of stress affecting the formation. The reason for this is that the pressure must have overcome the normal stresses on the fractures (Delaney et al., 1986), where the normal stress acting on the plane normal to the unit vector $\mathbf{v}$ under the stress tensor $\boldsymbol{\sigma}$ is written as $\mathbf{v}^\top\boldsymbol{\sigma}\mathbf{v}$. It is seen that normal stress has orthorhombic symmetry with respect to the principal stress planes (Fig. 12). Therefore, elongated clusters and girdles made by the poles to those structures must be identified by clustering for paleostress analysis, because the orthorhombic symmetry of such clusters reflects that of a stress tensor (Baer et al., 1994; Jolly and Sanderson, 1997; Yamaji et al., 2010). There is no need to distinguish the elongated clusters with the common center in Fig. 8 for people who aim only at clustering fracture orientations. However, we have to distinguish such clusters so that we can detect the stresses indicated by the clusters. Therefore, we employed Bingham distributions, which have probability distributions with orthorhombic symmetry (Fig. 1).

The present method is not the first to make use of an information criterion to determine the number of partitions in the clustering of orientation data. This has been done by Hammah

and Curran (1998), Peel et al. (2001) and Dortet-Bernadet and Wicker (2008), but the clusters captured by their methods did not always have orthorhombic symmetry. The method of Hammah and Curran (1998) detected circular clusters. Accordingly, those methods are not convenient for paleostress analysis. Fitting a mixed Bingham distribution combined with an information criterion is suitable for determining stresses from heterogeneous orientation data.

7. Conclusion

For geotechnical modeling and understanding brittle tectonics, we propose a clustering technique for heterogeneous orientation data by means of the mixed Bingham distribution. Bingham distributions are so flexible that they can describe not only the elliptical clusters but also the girdles of the orientations. In addition, paleostress analysis is straightforward when the distributions are fitted to the orientations of tensile fractures. If the clusters have little overlap, it is easy for our method to separate them and to determine the size and the aspect ratio of the clusters. In addition, elongated clusters with a common maximum concentration orientation can be separated, if a few conditions are satisfied.

Tests with artificial data sets demonstrated that the number of Bingham components was successfully estimated by means of Bayesian information criterion (BIC), if Bingham components were identified from heterogeneous orientation data. The method was applied to a dike swarm near a Miocene cauldron in Southwest Japan, and detected two paleostress states.

Acknowledgments

We are grateful to Tom Blenkinsop and an anonymous reviewer, whose comments and suggestions were very helpful for improving the manuscript. We thank Takeyoshi Yoshida for his comment on the magmatism in the Ishizuchi area. This work was partly supported by the grants 22340150 and 21740364 from JSPS.

Appendix A. Parameter space

For the EM algorithm to work, a parameter space was defined to indicate the parameters of a Bingham component, **E** and **K**. There are two necessary conditions for this space. First, the every point in the space should have a one-to-one correspondence with the pair, **E** and **K**. Second, distances in the space should not be affected by the coordinate rotations in the physical space to guarantee the accuracy and resolution of the method to be free from the choice of a coordinate system. To meet these demands, we modified the 5-dimensional stress space of Sato and Yamaji (2006).

A point in this modified space was represented by the position vector

$$\mathbf{x} = \rho\boldsymbol{\xi} \tag{5}$$

where ρ and $\boldsymbol{\xi}$ are distance from the origin of the 5-dimensional space and the unit vector indicating a ray from it. The combination of the parameters $\{\mathbf{E}, \kappa_1, \kappa_2\}$ is transformed to $\mathbf{x}$ as follows.

In this work, we use the distance,

$$\rho = \sqrt{\kappa_1^2 + \kappa_1\kappa_2 + \kappa_2^2}. \tag{6}$$

The right-hand side of this equation is the square root of the second basic invariant of the tensor, $\mathrm{diag}(-\kappa_1 - \kappa_2, \kappa_2, \kappa_1)$, which is one of the simplest deviatoric tensors composed from κ_1 and κ_2. The second basic invariant is generally a measure of anisotropy. By definition, the concentration parameters satisfy $\kappa_1 \le \kappa_2 \le 0$. Thus, in case of $\kappa_1 = 0$, we obtain $\mathbf{x} = \mathbf{0}$ from Eqs. (5) and (6).

In case of $\kappa_1 \neq 0$, we use the ratio, $r \equiv \kappa_2/\kappa_1$, to calculate $\boldsymbol{\xi}$. This ratio has a value between 0 and 1. And, we use the deviatoric tensor,

$$\boldsymbol{\varsigma} = \mathbf{E}\left[\frac{\mathrm{diag}(2-r, 2r-1, -r-1)}{\sqrt{3r^2 - 3r + 3}}\right]\mathbf{E}^\top. \tag{7}$$

Let ς_{ij} be the ijth component of this tensor. Since the trace of $\boldsymbol{\varsigma}$ is invariant under the rotation by the action of $\mathbf{E}$ in Eq. (7), the equation

$$\varsigma_{11} + \varsigma_{22} + \varsigma_{33} = 0, \tag{8}$$

holds independent of $\mathbf{E}$. Then, the components of the ray are given by

$$\begin{cases} \xi_1 = -\left(\frac{\sqrt{2}}{4} + \frac{\sqrt{6}}{12}\right)\varsigma_{11} + \left(\frac{\sqrt{2}}{4} - \frac{\sqrt{6}}{12}\right)\varsigma_{22} + \frac{1}{\sqrt{6}}\varsigma_{33} \\ \xi_2 = \left(\frac{\sqrt{2}}{4} - \frac{\sqrt{6}}{12}\right)\varsigma_{11} - \left(\frac{\sqrt{2}}{4} + \frac{\sqrt{6}}{12}\right)\varsigma_{22} + \frac{1}{\sqrt{6}}\varsigma_{33} \\ \xi_3 = \varsigma_{23}, \quad \xi_4 = \varsigma_{31}, \quad \xi_5 = \varsigma_{12}. \end{cases} \tag{9}$$

This linear equation was originally introduced to fault-slip analysis by Sato and Yamaji (2006). In terms of Eqs. (5), (6) and (9), we obtain $\mathbf{x}$ corresponding to $\{\mathbf{E}, \kappa_1, \kappa_2\}$.

On the other hand, given a point $\mathbf{x}$ in the parameter space, the parameters $\mathbf{E}$, κ_1 and κ_2 are calculated as follows. In case of $\mathbf{x} = \mathbf{0}$, we immediately obtain $\kappa_1 = \kappa_2 = 0$. This means a uniform orientation distribution in the physical space. Therefore, we do not need to calculate $\mathbf{E}$. In case of $\mathbf{x} \neq \mathbf{0}$, we have $\rho = |\mathbf{x}|$ and $\boldsymbol{\xi} = \mathbf{x}/\rho$. It follows from Eqs. (8) and (9) that

$$\begin{cases} \varsigma_{11} = -\left(\frac{1}{\sqrt{2}} + \frac{1}{\sqrt{6}}\right)\xi_1 + \left(\frac{1}{\sqrt{2}} - \frac{1}{\sqrt{6}}\right)\xi_2 \\ \varsigma_{22} = \left(\frac{1}{\sqrt{2}} - \frac{1}{\sqrt{6}}\right)\xi_1 - \left(\frac{1}{\sqrt{2}} + \frac{1}{\sqrt{6}}\right)\xi_2 \\ \varsigma_{33} = \sqrt{2/3}\,(\xi_1 + \xi_2) \\ \varsigma_{23} = \varsigma_{32} = \xi_3, \quad \varsigma_{31} = \varsigma_{13} = \xi_4, \quad \varsigma_{12} = \varsigma_{21} = \xi_5, \end{cases}$$

where ξ_i is the ith component of $\boldsymbol{\xi}$. Then, $\mathbf{E}$ and r are obtained by solving the eigenproblem of $\boldsymbol{\varsigma}$ (Eq. 7). That is, $\mathbf{E}$ is composed as $\mathbf{E} = (\mathbf{e}_1, \mathbf{e}_2, \mathbf{e}_3)$, where $\mathbf{e}_i$ is the 3×1-matrix representing the eigenvector corresponding the ith eigenvalue. Let $\varsigma_1 \ge \varsigma_2 \ge \varsigma_3$ be the eigenvalues. Then, we obtain $r = (\varsigma_2 - \varsigma_3)/(\varsigma_1 - \varsigma_3)$. Substituting $\kappa_2 = r\kappa_1$ into Eqs. (6) we have $\rho^2 = (r^2 + r + 1)\kappa_1^2$. Since κ_1 must be negative in sign, we obtain

$$\kappa_1 = -\rho/\sqrt{r^2 + r + 1}. \tag{10}$$

Using Eq. (10) we finally get $\kappa_2 = r\kappa_1$.

References

Ahmadhadi, F., Daniel, J.-M., Azzizadeh, M., Lacombe, O., 2008. Evidence for pre-olding vein development in the Oligo-Miocene Asmari Formation in the Central Zagros Fold Belt, Iran. Tectonics 27, T1016. doi:10.1029/2006TC001978.

André, A.-S., Sausse J., Lespinasse M., 2001. New approach for the quantification of paleostress magnitudes: application to the Soultz vein system (Rhine graben, France). Tectonophysics 336, 215–231. doi:10.1016/S0040-1951(01)00103-2.

Baer, G. Beyth, M., Reches, Z., 1994. Dikes emplaced into fractured basement, Timna Igneous Complex, Israel. Journal of Geophysical Research 99, 24039–24051. doi:10.1029/94JB02161.

Banerjee, A., Dhillon, I.S., Ghosh, J., Sra, S., 2005. Clustering on the Unit Hypersphere using von Mises-Fisher Distributions. Journal of Machine Learning Research 6, 1345–1382.

Bingham, C., 1974. An antipodally symmetric distribution on the sphere. Annals of Statistics 2, 1201–1225. doi:10.1214/aos/1176342874.

Bishop, C.M., 2006. Pattern Recognition and Machine Learning. Springer, New York.

Chen, X., Yang, Q., Qiu, K.B., Feng, J.L., 2008. An anisotropic strength criterion for jointed rock masses and its application in wellbore stability analyses. International Journal for Numerical and Analytical Methods in Geomechanics 32, 607–631. doi:10.1002/nag.638.

Delaney, P.T., Pollard, D.D., Zioney, J.I., McKee, E.H., 1986. Field relations between dikes and joints: emplacement processes and paleostress analysis. Journal of Geophysical Research 91, 4920–4983. doi:10.1029/JB091iB05p04920.

Dortet-Bernadet, J.-L., Wicker, N., 2008. Model-based clustering on the unit sphere with an illustration using gene expression profiles. Biostatistics 9, 66–80. doi:10.1093/biostatistics/kxm012.

Etchecopar, A., Vasseur, G., Daignieres, M., 1981. An inverse problem in microtectonics for the determination of stress tensors from fault striation analysis. Journal of Structural Geology 3, 51–65. doi:10.1016/0191-8141(81)90056-0.

Hammah, R.E., Curran, J.H., 1998. Fuzzy cluster algorithm for the automatic identification of joint sets. International Journal of Rock Mechanics and Mining Sciences 35, 889–905. doi:10.1016/S0148-9062(98)00011-4.

Hammah, R.E., Curran, J.H., 1999. On distance measure for the fuzzy k-means algorithm for joint data. Rock Mechanics and Rock Engineering 32, 1–27. doi:10.1007/s006030050041.

Jimenez-Rodriguez, R., Sitar, N., 2006. A spectral method for clustering of rock discontinuity sets. International Journal of Rock Mechanics and Mining Sciences 43, 1052–1061. doi:10.1016/j.ijrmms.2006.02.003.

Jolly, R.J.H., Sanderson, D.J., 1997. A Mohr circle construction for the opening of a pre-existing fracture. Journal of Structural Geology 19, 887–892. doi:10.1016/S0191-8141(97)00014-X.

Klose, C.D., Seo, S., Obermayer, K., 2005. A new clustering approach for partitioning directional data. International Journal of Rock Mechanics and Mining Geology 42, 315–321. doi:10.1016/j.ijrmms.2004.08.011.

Kowallis, B.J., Wang, H.F., Jang, B.-A., 1987. Healed microcrack orientations in granite from Illinois borehole UPH-3 and their relationship to the rock's stress history. Tectonophysics 135, 297–306. doi:10.1016/0040-1951(87)90114-4.

Kobayashi, Y., 1979. Early and Middle Miocene dike swarms and regional tectonic stress field in the Southwest Japan. Journal of Volcanological Society of Japan, 2nd Series, 24, 203–212.

Kusuhashi, N., Yamaji, A., 2001. Miocene tectonics of SW Japan as inferred from the Kuma Group, Shikoku. Journal of Geological Society of Japan 107, 26–40.

Lespinasse, M., Pécher, A., 1986. Microfracturing and regional stress field: a study of the preferred orientations of fluid-inclusion planes in a granite from the Massif Central, France. Journal of Structural Geology 8, 169—177. doi:10.1016/0191-8141(86)90107-0.

Love, J.J., 2007. Bingham statistics. In: Gubbins, D., Herrero-Bervira, E. (Eds.), Encyclopedia of Geomagnetism and Paleomagnetism, Springer, Dordrecht. 45–47.

MacQueen, J.B., 1967. Some methods for classification and analysis of multivariate observations. Proceedings of Fifth Berkeley Symposium on Mathematical Statistics and Probability, Volume I, pp. 281–297.

Marcotte, D., Henry, E., 2002. Automatic joint set clustering using a mixture of bivariate normal distributions. International Journal of Rock Mechanics and Mining Sciences 39, 323–334. doi:10.1016/S1365-1609(02)00033-3.

Mazzarini, F., Isola, I., 2007. Hydraulic connection and fluid overpressure in upper crustal rocks: Evidence from the geometry and spatial distribution of veins at Botrona quarry, southern Tuscany, Italy. Journal of Structural Geology 29, 1386–1399. doi:10.1016/j.jsg.2007.02.016.

Nagai, K., Horikoshi, K., 1955. Geology of the neighborhood of Kuromoritoge, Onsen-gun, Ehime-ken. Ehime Daigaku Kiyo Shizen Kagaku C2, 57–70.

Nelder, J.A., Mead, R., 1965. A simplex method for function minimization. Computer Journal 7, 308–313. doi:10.1093/comjnl/7.4.308.

Nemcok, M., Lisle, R.J., 1995. A stress inversion procedure for polyphase fault/slip data sets. Journal of Structural Geology 17, 1445–1453. doi:10.1016/0191-8141(95)00040-K.

Ohtsu, H., Hotta, Y., Saegusa, H., Ijiri, Y., Onoe, H., 2008. An application of risk assessment method of water inrush in fractured rock masses to actual underground construction project. Doboku Gakkai Ronbunshuu F64, 353–368.

Panda, B.B., Kultilake, P.H.S.W., 1999. Effect of joint geometry and transmissivity on jointed rock hydraulics. Journal of Engineering Mechanics 125, 41–50. doi:10.1061/(ASCE)0733-9399(1999)125:1(41).

Pecher, A., 1989. SCHMIDTMAC: A program to display and analyze directional data. Computers & Geosciences 15, 1315–1326. doi:10.1016/0098-3004(89)90095-2.

Peel, D., Whiten, W.J., McLachlan, G.J., 2001. Fitting mixtures of Kent distributions to aid in joint set identification. Journal of the American Statistical Association 96, 56–63. doi:10.1198/016214501750332974.

Press, W.H., Teukolsky, S.A., Vettering, W.T., Flannery, B.P., 2007. Numerical Recipies: The Art of Scientific Computing, 3rd Edition. Cambridge University Press, Cambridge.

Priest, S.D., 1993. Discontinuity Analysis for Rock Engineering. Chapman and Hall, London.

Sato, K., 2006. Incorporation of incomplete fault-slip data into stress tensor inversion. Tectonophysics 421, 319–330. doi:10.1016/j.tecto.2006.05.004.

Sato, K., Yamaji, A., 2006. Embedding stress difference in parameter space for stress tensor inversion. Journal of Structural Geology 28, 957–971. doi:10.1016/j.jsg.2006.03.004.

Schwarz, G., 1978. Estimating the dimension of a model. Annals of Statistics 6, 461–464. doi:10.1214/aos/1176344136.

Shan, Y., Suen, H., Lin, G., 2003. Separation of polyphase fault/slip data: An objective-function algorithm based on hard division. Journal of Structural Geology 25, 829–840. doi:10.1016/S0191-8141(02)00082-2.

Shanley, R.J., Mahtab, M.A., 1976. Delineation and analysis of clusters in orientation data. Mathematical Geology 8, 9–23. doi:10.1007/BF01039681.

Tan, P.-N., Steibach, M., Kumar, V., 2005. Introduction to Data Mining. Addison-Wesley, Boston.

Wallbrecher, E., 1978. Ein Cluster-Verfahren zure richtungsstatistischen Analyse tektonischer Daten. Geologische Rundschau 67, 840–857. doi:10.1007/BF01983240.

Whitaker, A.E., Engelder, T., 2005. Characterizing stress fields in the upper crust using joint orientation distributions. Journal of Structural Geology 27, 1778–1787. doi:10.1016/j.jsg.2005.05.016.

Yamaji, A., 2000. Multiple inverse method: a new technique to separate stresses from heterogeneous fault-slip data. Journal of Structural Geology 22, 441–452. doi:10.1016/S0191-8141(99)00163-7.

Yamaji, A., Otsubo, M., Sato, K., 2006. Paleostress analysis using the Hough transform for separating stresses from heterogeneous fault-slip data. Journal of Structural Geology 28, 980–990. doi:10.1016/j.jsg.2006.03.016.

Yamaji, A., Sato, K., 2006. Distances for the solutions of stress tensor inversion in relation to misfit angles that accompany the solutions. Geophysical Journal International 167, 913–942. doi:10.1111/j.1365-246X.2006.03188.x

Yamaji, A., Sato, K., Tonai, S., 2010. Stochastic modeling for the stress inversion of vein orientations: paleostress analysis of Pliocene epithermal veins in southwestern Kyushu, Japan. Journal of Structural Geology, in press. doi:10.1016/j.jsg.2010.07.001.

Yamaji, A., Yoshida, T., 1998. Multiple tectonic events in the Miocene Japan arc: the Heike microplate hypothesis. Journal of Mineralogy, Petrology and Economic Geology 93, 389–408. doi:10.2465/ganko.93.389.

Yoshida, T., 1984. Tertiary Ishizuchi Cauldron, Southwestern Japan Arc, formation by ring fracture subsidence. Journal of Geophysical Research 89, 8502–8510. doi:10.1029/JB089iB10p08502.

Yoshida, T., Murata, M., Yamaji, A., 1993. Formation of Ishizuchi cauldron and Miocene tectonics. Memoir of the Geological Society of Japan 42, 297–349.